

Dual-wavelength image-plane digital holography for dynamic measurement

Yu Fu^{a,b,*}, Giancarlo Pedrini^a, Bryan M. Hennelly^c, Roger M. Groves^a, Wolfgang Osten^a

^a Institut für Technische Optik, Universität Stuttgart, Pfaffenwaldring 9, D-70569, Stuttgart, Germany

^b Department of Mechanical Engineering, National University of Singapore, 10 Kent Ridge Crescent, 119260 Singapore

^c Department of Computer Science, National University of Ireland, Maynooth, County Kildare, Ireland

ARTICLE INFO

Article history:

Received 22 February 2008

Received in revised form

15 September 2008

Accepted 12 October 2008

Available online 20 November 2008

Keywords:

Digital holography

Two-wavelength

Windowed Fourier analysis

Vibration measurement

Phase retrieval

ABSTRACT

A dual-wavelength image-plane digital holography, combined with a windowed Fourier analysis, is presented for dynamic measurement of a vibrating object. In order to expand the range of the velocity measurement, the object is simultaneously illuminated by two lasers with different wavelengths. A sequence of digital holograms of a vibrating object is captured by a CCD camera and two wrapped phase maps are retrieved from each digital hologram. At each instant, a new phase distribution with a synthetic wavelength is obtained by subtracting these two wrapped phase maps. A windowed Fourier analysis is then applied spatially and temporally to retrieve the high-precision displacement and velocity of the tested object. Experimental results show the requirement on the camera capture frequency is reduced by the proposed method.

© 2008 Elsevier Ltd. All rights reserved.

1. Introduction

Since 1960s, various optical non-contact techniques have been applied for whole-field, non-contact dynamic measurement. Among them, the time-average method [1] is a typical technique for objects vibrating at a sinusoidal frequency whose period is many times smaller than the exposure time. The use of a twin-cavity double-pulsed laser in interferometry [2] has also been reported as an alternative to obtain transient parameters. Because of the rapid development of high-speed cameras, it is possible to record a sequence of interferograms with high capturing rates. High-speed phase-shifting [3] and temporal phase analysis [4,5] were techniques introduced to retrieve the phase variation during the deformation or vibration of the objects. The former technique requires a high-speed phase shifter synchronized with a high-speed camera, while the latter technique analyzes each pixel of the interferograms independently as a function of time. Different processing algorithms including phase scanning [6], Fourier transform (FT) [7], windowed Fourier transform (WFT) [8,9] and continuous wavelet transform (CWT) [10,11] have been applied temporally or spatially to retrieve the phase from these two techniques.

In the past decade, a novel computer-aided optical technology, digital holography [12], has been successfully applied to different

types of measurement. With a high-resolution CCD or CMOS sensor, one can record holograms directly with a camera and reconstruct the object digitally by computer simulation. The phase of the object can be retrieved from the digital reconstruction of one hologram. This advantage makes digital holography more suitable for dynamic measurement. In addition, no phase ambiguity problem exists in the further processing of the reconstructed phase. Different dynamic measurement techniques based on digital holography combined with a pulsed laser [13], a time-average method [14], and a temporal analysis [15] have been reported. A previous report [16] described a method for the measuring kinematic parameters of a vibrating object by image-plane digital holography. Digital holograms of a vibrating object were recorded on a high-speed sensor and the phase of the wavefront, recorded at different instants, was calculated from the recorded intensity using a two-dimensional (2-D) FT method. By processing the phase maps with a one-dimensional (1-D) WFT in the temporal domain, it is possible to obtain the instantaneous displacement, velocity and acceleration of the vibrating object.

One problem involved in dynamic measurements is that the imaging rate of the camera should be high enough so that the phase change on each pixel, between two adjacent images, should be less than π . This is equivalent to the path-length change of $\lambda/2$. It is impossible to bypass the Nyquist sampling theorem. However, we can enlarge the measurement range by two-wavelength interferometry (TWI) [17,18]. Different types of TWI have been reported during the past several decades. The phases at a synthetic wavelength have been determined from the

* Corresponding author at: Department of Mechanical Engineering, National University of Singapore, 10 Kent Ridge Crescent, 119260 Singapore.

E-mail address: fuyuoptics@gmail.com (Y. Fu).

difference between two phases at a single wavelength by the use of different methods, such as the heterodyne technique [19], the time-multiplexed technique [20], the phase-shifting technique [21], the three-color method [22], the sinusoidal phase-demodulated technique [23,24], the fractional fringe technique [25] or the Fourier-transform method [26]. A typical application of TWI is the measurement of a surface profile with height steps [27]. The concept of TWI can also be used with digital holography for surface profiling where the phase at single wavelength can be reconstructed from separately recorded digital holograms [28,29]. However, it is not suitable for dynamic measurement because two holograms need to be recorded and reconstructed individually. In this paper, we propose TWI combined with image-plane digital holography to achieve a dynamic measurement on a vibrating object. The object was simultaneously illuminated by two lasers with different wavelengths, and a sequence of digital holograms was captured by a CCD camera. For each instant, two wrapped phase maps were reconstructed from one digital hologram [30,31]. A new phase distribution with a synthetic wavelength was then obtained by subtracting these two wrapped phase maps. However, the new phase map is much noisier [32], and needed a robust algorithm to retrieve the temporal phase values and the phase derivatives. In this application, a windowed Fourier analysis was applied spatially and temporally to retrieve the instantaneous displacement and velocity of a vibrating object.

2. Theoretical analysis

2.1. Two-wavelength image-plane digital holography

A schematic layout of an image-plane digital holography configuration, sensitive to out-of-plane displacement, is shown in Fig. 1. Two lasers with different wavelengths are used. Light from the first laser is split into an object beam and a reference beam. This object beam illuminates a vibrating specimen with a diffuse surface along a direction \mathbf{e}_{i1} . Some light is scattered in the observation direction \mathbf{e}_o where an image-plane hologram is formed on the CCD sensor, as a result of the interference between the reference beam and the object beam. An aperture is put immediately behind the imaging lens to limit the spatial frequencies of the interference pattern. The reference beam is introduced by a single-mode optical fiber and diverges toward the CCD sensor from a point close to the aperture. Let $R_1(x,y)$ and $U_1(x,y)$ denote the reference and object waves of light from the first laser. The intensity recorded on the detector can be expressed as

$$I_1(x,y) = |R_1(x,y)|^2 + |U_1(x,y)|^2 + R_1(x,y)U_1^*(x,y) + R_1^*(x,y)U_1(x,y) \quad (1)$$

where * denotes the complex conjugate. The maximum spatial frequency in the hologram is given by

$$f_{1\max} = \frac{2}{\lambda_1} \sin\left(\frac{\theta_{1\max}}{2}\right) \quad (2)$$

where λ_1 is the wavelength of the first laser and $\theta_{1\max}$ is the maximum angle between the object and the reference beams. The condition $f_{1\max} < 1/(2\Delta)$ should be satisfied over the full area of the CCD sensor, and Δ denotes the pixel size of the camera. The last two terms in Eq. (1) contain information of the amplitude and phase of the object wave. This information can be obtained by spatial filtering of the Fourier spectrum [16]. After an inverse FT, the complex amplitude of the wavefront $U_1(x,y)$ is obtained.

Similarly a second different laser wavelength is used to generate a second interferogram on the CCD sensor. When these two lasers simultaneously illuminate the object and the detector,

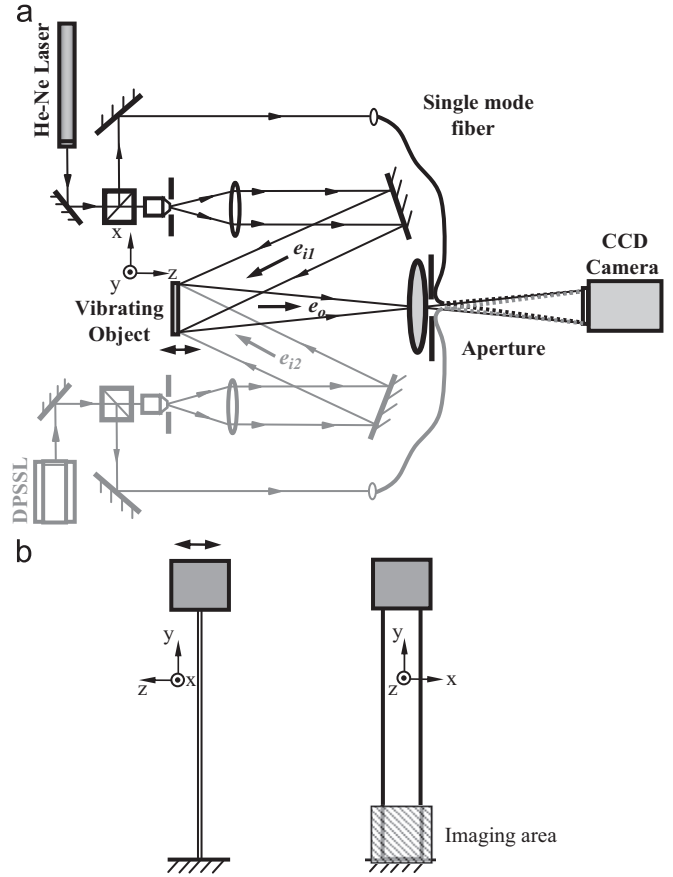


Fig. 1. (a) Schematic layout of the experimental setup; (b) the testing vibrating cantilever beam and the imaging area.

the two interferograms will be superimposed on the CCD sensor and one digital hologram containing information about these two interferograms will be obtained. Fig. 2(a) shows a typical digital hologram captured by the CCD camera. With a proper selection of the aperture size and a careful adjustment of the two fiber-end positions, it is possible to separate the spectrums of two superimposed holograms in the frequency domain. Fig. 2(b) shows the Fourier spectrum of the hologram in Fig. 2(a). The selection of different filtering windows yields two complex amplitudes of the wavefronts $U_1(x,y)$ and $U_2(x,y)$ after the inverse FT. In our experiment, a series of digital holograms is captured during the vibration of the specimen. Hence, two series of complex amplitudes are obtained with different wavelengths.

In dynamic measurement, the displacement of an object gives a change in the phase of the object beam. The relationship between the phase change $\Delta\phi$ and the out-of-plane displacement z is given by

$$\Delta\phi = \frac{2\pi z}{\lambda} \cdot \mathbf{S} \quad (3)$$

where $\mathbf{S} = \mathbf{e}_i - \mathbf{e}_o$ and \mathbf{S} is the sensitivity vector given by the geometry of the setup, and \mathbf{e}_i and \mathbf{e}_o are the unit vectors of illumination and observation, respectively. For this case, the phase changes at different wavelengths are given by

$$\Delta\phi_N = 2 \cos\left(\frac{\alpha_N}{2}\right) \frac{2\pi z}{\lambda_N} = \frac{2\pi z}{\lambda_{eqN}} \quad (4)$$

where $N = 1, 2$; α_1 and α_2 are the angles between the observation direction and the illumination directions with different lasers. $\lambda_{eqN} = \lambda_N / (2\cos(\alpha_N/2))$ ($N = 1, 2$) are the equivalent wavelengths for the out-of-plane displacement measurement when the

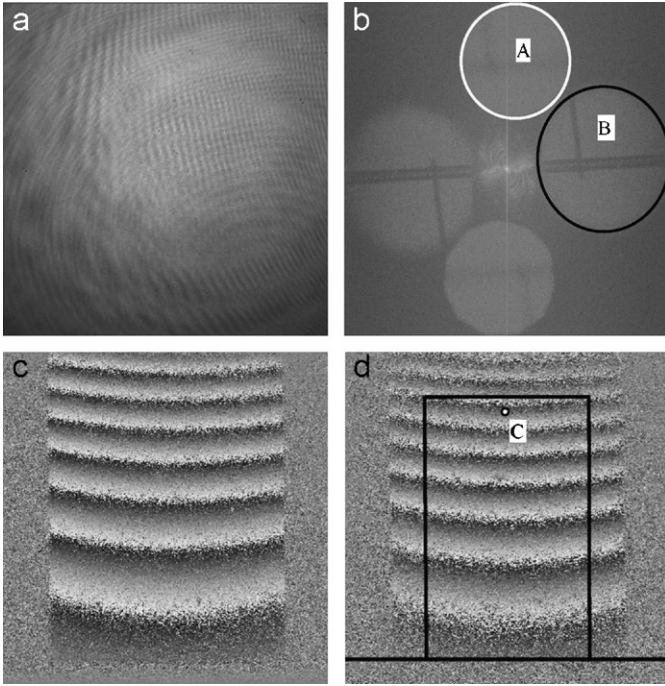


Fig. 2. (a) Typical digital hologram obtained by illumination from two lasers; (b) spectrum of the digital hologram obtained; (c) typical original wrapped phase map with $\lambda_1 = 633$ nm; (d) typical original wrapped phase map with $\lambda_2 = 523$ nm, and the selected area to process.

illumination direction is considered. The phase difference between two digital holograms recorded at instants t_1 and t_m can be calculated by

$$\Delta\phi_N = \arctan \frac{\text{Im}(U_N(x, y; t_m) \cdot U_N^*(x, y; t_1))}{\text{Re}(U_N(x, y; t_m) \cdot U_N^*(x, y; t_1))} \quad (5)$$

where $N = 1$ and 2 , Re and Im denote the real and imaginary parts respectively of the complex value. Fig. 2(c and d) show a typical instantaneous phase difference on a vibrating cantilever beam for two different laser wavelengths, respectively. At each instant t_m , a new phase distribution is calculated directly by the subtraction of these two wrapped phases:

$$\Phi = \begin{cases} \Delta\phi_1 - \Delta\phi_2 & \text{if } \Delta\phi_1 \geq \Delta\phi_2 \\ \Delta\phi_1 - \Delta\phi_2 + 2\pi & \text{if } \Delta\phi_1 < \Delta\phi_2 \end{cases} \quad (6)$$

where $0 \leq \Phi < 2\pi$. This phase map is equivalent to a phase distribution of an out-of-plane displacement measurement with a synthetic wavelength Λ , where

$$\Lambda = \frac{\lambda_{\text{eq1}} \lambda_{\text{eq2}}}{|\lambda_{\text{eq1}} - \lambda_{\text{eq2}}|} \quad (7)$$

In practice, this phase map contains much more noise than the conventional image-plane digital holography. Normally it is impossible to retrieve the displacement by direct temporal unwrapping. In this application, a windowed Fourier analysis is applied to evaluate the displacement and velocity on a vibrating object.

2.2. Windowed Fourier analysis

A 1-D WFT and the inverse windowed Fourier transform (IWFT) can be written as [33]

$$Sf(u, \xi) = \int_{-\infty}^{+\infty} f(t)g_{u, \xi}^*(t) dt \quad (8)$$

and

$$f(t) = \frac{1}{2\pi} \int_{-\infty}^{+\infty} \int_{-\infty}^{+\infty} Sf(u, \xi)g_{u, \xi}(t) d\xi du \quad (9)$$

where $f(t)$ is the original signal; $Sf(u, \xi)$ denotes the spectrum of WFT and $g_{u, \xi}(t)$ is the WFT kernel, which can be expressed as

$$g_{u, \xi}(t) = g(t - u) \exp(j\xi t) \quad (10)$$

The window $g(t)$ is usually chosen as a Gaussian function:

$$g(t) = \exp(-t^2/2\sigma^2) \quad (11)$$

which permits the best time-frequency localization in analysis. The parameter σ controls the extension of $g(t)$. We convert the obtained series of wrapped phase Φ to an exponential signal $C_p = \exp(j \cdot \Phi)$. The WFT of this complex signal will be [33]

$$SC_p(u, \xi) = \frac{\sqrt{s}}{2} A_p \exp(j[\Phi(u) - \xi u]) (\hat{g}(s[\xi - \Phi'(u)]) + \varepsilon(u, \xi)) \quad (12)$$

where u and ξ represent the time shift and frequency, respectively, and scaling factor s is a function of σ , who controls the window size. A_p is the modulus of C_p and is equal to one in this case. $\Phi'(u)$ is defined as the instantaneous frequency of the signal, which is proportional to the velocity in our case. $\varepsilon(u, \xi)$ is a corrective term which can be neglected if $A_p(u)$ and $\Phi'(u)$ have small relative variations over the support of window g . $\hat{g}(\omega)$ denotes the FT of $g(t)$, which is also a Gaussian function. The trajectory of the maximum $|SC_p(u, \xi)|^2$ on the u - ξ plane is called a windowed Fourier 'ridge'. Since $|\hat{g}(\omega)|$ is maximum at $\omega = 0$, and if ε is negligible, $|SC_p(u, \xi)|^2$ reaches maximum when

$$\xi(u) = \Phi'(u) \quad (13)$$

A WFT maps a 1-D temporal signal to a 2-D time-frequency plane, and extracts the signal's instantaneous frequency. Compared with Fourier filtering, it is a more effective technique for the removal of noise within the frequency band of the signal, but at the cost of long processing time. The WFT can be extended to a 2-D case to extract the phase and phase derivatives on the x - y plane, and to the three-dimensional (3-D) case of the x - y - t axes. The details of the WFT technique are given in Refs. [8,34]. In this case, the phase nonlinearity is more obvious in the t -axis, but milder in the x - y domain. Thus in a 3-D process, a small parameter σ should be selected for the time axis, but a large σ for the spatial domain.

3. Experimental illustration

Fig. 1 shows the experimental setup for the measurements. The specimen tested in this study was a copper cantilever beam with a diffuse surface. A weight is fixed at the free-end of the beam. The distance between the weight and the clamping end was 80 mm. The width and thickness of the beam were 10 and 0.3 mm, respectively. The natural frequency of the beam was around 2 Hz. The first laser used was a He-Ne laser with a power of 15 mW and with a wavelength of $\lambda_1 = 632.8$ nm. The second laser used was a diode-pumped solid state laser (DPSSL, Laser Technologies, Model no. MSL532-20) with a wavelength λ_2 of 532 nm. The cantilever beam was simultaneously illuminated from an angle of $\alpha_1 = 17.9^\circ$ by the He-Ne laser and from an angle of $\alpha_2 = 16.7^\circ$ by the DPSSL. Two single-mode fibers directed the reference beams with different wavelengths toward the CCD sensor from points close to the aperture, and the two interferograms generated by the red and green lasers were superimposed on the camera sensor. The camera used was a PULNIX TM-1001 with an imaging rate of 15 fps, a pixel size of $9.0 \times 9.0 \mu\text{m}^2$ and a resolution of 992×1018 pixels. Fig. 1(b) also shows the imaging area of the beam, and

calibration shows 1 mm on the beam occupies 72 pixels on the image.

It is worth noting that for the illumination directions of two lasers it was not necessary to illuminate from two different sides as shown in Fig. 1(a). We use the configuration because only the out-of-displacement is concerned in this application. The illuminations could be combined with a beam splitter so that the object is illuminated from one side. The angles α_1 and α_2 are other factors that can adjust the value of the synthetic wavelength. However, an accurate measurement of these two angles is sometimes difficult to achieve in the experiment. In many cases, a calibration of the synthetic wavelength is necessary by shifting an object in z-direction with a known distance and measuring the phase change by the proposed method. In our application, the synthetic wavelength was evaluated as $\lambda = 3342$ nm.

4. Results and discussion

One hundred and twenty holograms are captured during an 8 s period. Fig. 2(b) shows a typical Fourier spectrum of digital holograms captured by the CCD camera. The shadow of the fiber ends can be observed on the spectrums of both digital holograms. When *filtering window A* is selected, the reconstructed phase difference between the two instants represents the out-of-plane displacement for the wavelength 632.8 nm (Fig. 2(c)). When *filtering window B* is selected, the reconstructed phase between the two instants is the result with wavelength of 532 nm (Fig. 2(d)). A slightly difference can be observed between these two wrapped phase maps. The first two rows of Fig. 3 also show series of phase maps with these two wavelengths in a consecutive sequence. Obviously the sampling points in the time axis are not enough, as the phase change between two adjacent frames are sometimes much more than π . However, by subtracting one wrapped phase from another at each instant using Eq. (6), a new series of wrapped phases can be obtained as shown in the third row of Fig. 3. These phase maps represent the out-of-displacement measurement with the synthetic wavelength of 3342 nm. The phase difference between the two adjacent frames is within the Nyquist frequency.

At each instant, the noise in the wrapped phase map with red and green lasers was different and could not be cancelled in the subtraction. Hence, the noise effect is more serious in the wrapped phase map with the synthetic wavelength. The wrapped phases were then converted to exponential phase signals and filtered by FT and WFT. The fourth row of Fig. 3 shows the result of 2-D Fourier filtering. It can be observed the Fourier filtering is not so effective, even when a small filtering window size is selected. However in the 2-D WFT, as the second derivative of the phase change Φ'' is small in spatial domain and a large Gaussian window size in x- and y- axis can be selected and the phase maps (shown in the fifth row of Fig. 3) are suitable for the further processing along the time axis. One hundred and twenty frames of filtered wrapped phase map were obtained. Fig. 4 shows the phase variation of point C [indicated in Fig. 2(d)] after 1-D temporal phase unwrapping. Figs. 5 and 6 respectively show 3-D plots of the displacement and velocity at different instants after a 3-D WFT. In this case, the Gaussian window sizes at different directions are selected as $\sigma_t = 2$ and $\sigma_x = \sigma_y = 15$, due to the large nonlinearity of phase variation in time axis, and mild variation is spatial domain. Instantaneous displacement and velocity distributions with good quality are obtained.

However, as the initial wrapped phases with different wavelengths were retrieved from one digital hologram, the aperture in Fig. 1 could not be too large, as the spectrums of different wavelengths should be separated in the frequency domain, as shown in Fig. 2(b). Hence the bandpass windows A and B are relatively smaller than used in normal image-plane digital holography (Ref. [16]). This corresponds to the increase in the speckle size and a reduction in the spatial resolution in the reconstructed wrapped phase maps (Fig. 2(c and d)). This means that the relative displacement on the testing object cannot be too large so that the fringe density in Fig. 2(c and d) is not too high. Otherwise, it would be impossible to retrieve the correct phase distribution after subtraction of the two initial wrapped phase maps. This makes the proposed method most suitable for measurements of a rigid-body vibration.

The signal obtained in optical dynamic measurement is a phase variation. TWI generates a large synthetic wavelength to enlarge the measurement range. Theoretically the smaller the

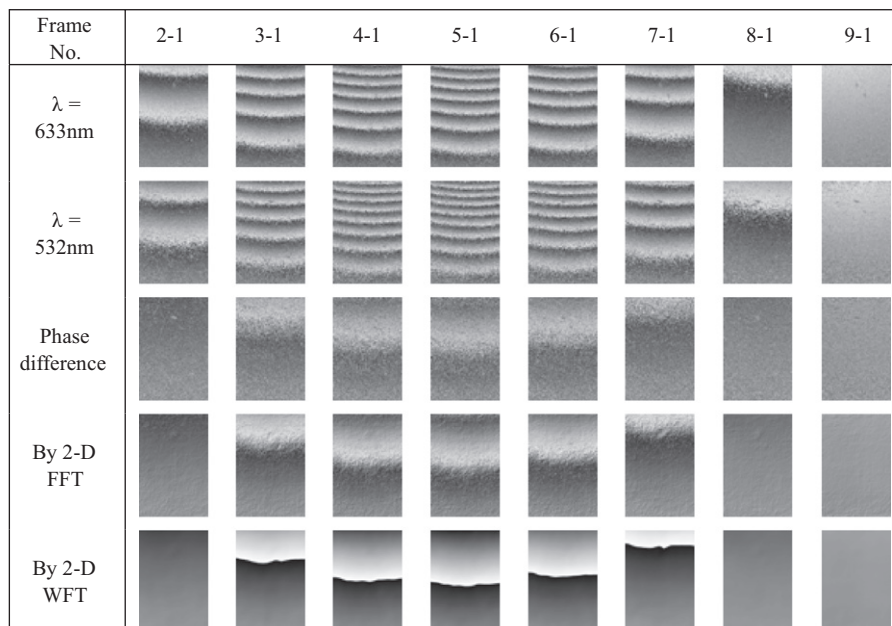


Fig. 3. Series of wrapped phase map obtained by (1) $\lambda_1 = 633$ nm; (2) $\lambda_2 = 523$ nm; (3) phase difference between the result of λ_1 and λ_2 ; (4) wrapped phase map after 2-D Fourier filtering; (5) wrapped phase map after 2-D windowed Fourier filtering.

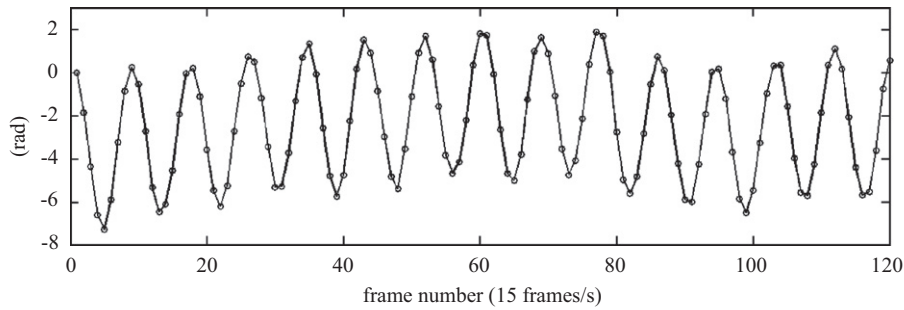


Fig. 4. Phase variation of point C with the synthetic wavelength $\lambda = 3342$ nm.

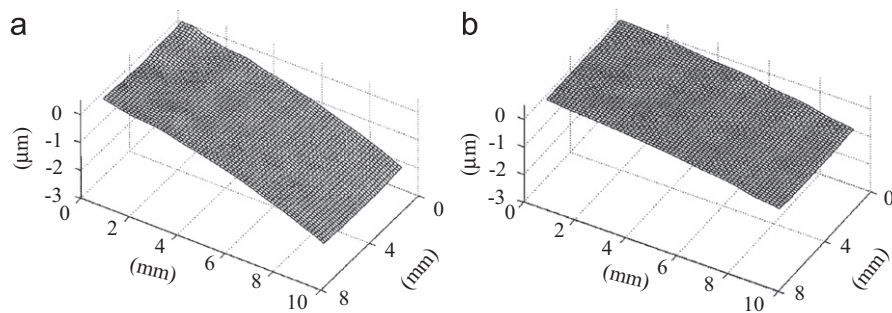


Fig. 5. 3-D plot of relative displacement between (a) frame nos. 1 and 5; (b) frame nos. 1 and 7 with imaging rate of 15 fps.

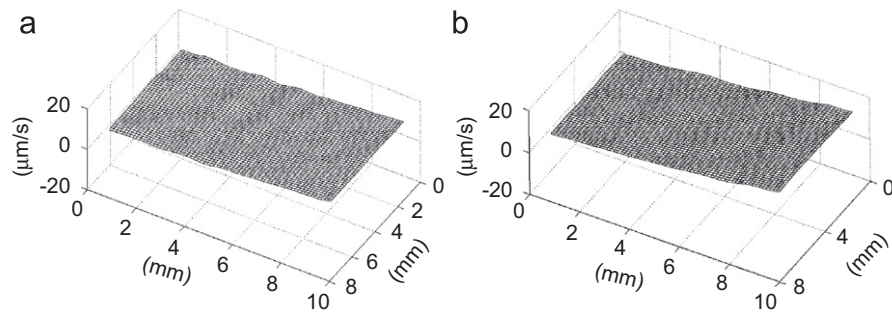


Fig. 6. 3-D plot of velocity at (a) frame no. 5 and (b) frame no. 7.

difference between two wavelengths, the larger the synthetic wavelength allowing a higher velocity to be detected. However, the requirement for a dynamic measurement is slightly different than that used for surface contouring (a 10^3 or 10^4 order of multiplication in wavelength is normally required). In dynamic measurement, a 10% difference in wavelength already increases the velocity measurement range by 10 times. Also vibration measurement is limited by Nyquist sampling frequency. At least two sampling points are required per vibration cycle. A large synthetic wavelength would not be helpful in this case. In addition, the speckle noise will affect the measurement seriously when the difference between λ_{eq1} and λ_{eq2} in Eq. (7) is too small. Thus a comprehensive judgment is necessary when the synthetic wavelength is selected.

5. Concluding remarks

In this paper we have presented a novel dual-wavelength image-plane digital holography on a vibration measurement. Two lasers with different wavelengths were used to illuminate the test

object simultaneously, and the two interferograms were superimposed on the CCD sensor. A sequence of digital holograms was captured by a CCD camera. At each instant, two wrapped phase maps were reconstructed from one digital hologram. The subtraction of these two phase maps yielded a new phase distribution with a synthetic wavelength. In this case, the synthetic wavelength was 5–6 times larger than that of the lasers used. This dramatically expanded the measurement range of velocity in the dynamic measurement. For a high-speed camera with the imaging rate of N fps, now it is possible to measure a vibration with the frequency of $N/2$, even if the vibration amplitude is large. Thus the sampling number needed for the large vibration amplitude can be dramatically reduced by the proposed method. By a further decrease of the aperture size and appropriate selection of the fiber positions it should be possible to include a third wavelength image in the image plane that is separated from the other two. This would allow a greater extension in the measurement range of the system. In addition, it is now possible to record interferograms with rates exceeding 1,00,000 frames per second (fps) due to the rapid development of high-speed digital recording devices. This will dramatically

increase the frequency range to be measured. Hence, digital holography presents high potential to do vibration measurement at different amplitude and frequency ranges.

Acknowledgements

Y. Fu gratefully acknowledges the financial support of the Alexander von Humboldt Foundation. This work is also supported by the German Science Foundation, DFG, Grant no. OS. 111/22-1, the MULTI-ENCODE project (006427 (SSPI)) funded by the European Union, and the National Science Foundation of China (NSFC) under Contract no. 10772171.

References

- [1] Nakadate S. Vibration measurement using phase-shifting time-average holographic interferometry. *Appl Opt* 1986;25(22):4155–61.
- [2] Farrant DI, Kaufmann GH, Petzing JN, Tyrer JR, Oreb BF, Kerr D. Measurement of transient deformations with dual-pulse addition electronic speckle-pattern interferometry. *Appl Opt* 1998;37(31):7259–67.
- [3] Huntley JM, Kaufmann GH, Kerr D. Phase-shifted dynamic speckle pattern interferometry at 1 kHz. *Appl Opt* 1999;38(31):6556–63.
- [4] Joenathan C, Franze B, Haible P, Tiziani HJ. Speckle interferometry with temporal phase evaluation for measuring large-object deformation. *Appl Opt* 1998;37(13):2608–14.
- [5] Kaufmann GH. Phase measurement in temporal speckle pattern interferometry using the Fourier transform method with and without a temporal carrier. *Opt Commun* 2003;217:141–9.
- [6] Li X, Tao G, Yang Y. Continual deformation analysis with scanning phase method and time sequence phase method in temporal speckle pattern interferometry. *Opt Laser Technol* 2001;33:53–9.
- [7] Takeda M, Ina H, Kobayashi S. Fourier-transform method of fringe-pattern analysis for computer-based topography and interferometry. *J Opt Soc Am* 1982;72:156–60.
- [8] Qian K. Two-dimensional windowed Fourier transform for fringe pattern analysis: Principles, applications and implementations. *Opt Laser Eng* 2007;45:304–17.
- [9] Qian K, Seah SH, Asundi A. Phase-shifting windowed Fourier ridges for determination of phase derivatives. *Opt Lett* 2003;28(18):1657–9.
- [10] Colonna de Lega X, Jacquot P. Interferometric deformation measurement using object induced dynamic phase shifting. In: *Proc SPIE*. Vol. 2782. 1996, pp. 169–79.
- [11] Fu Y, Tay CJ, Quan C, Chen LJ. Temporal wavelet analysis for deformation and velocity measurement in speckle interferometry. *Opt Eng* 2004;43(11):2780–7.
- [12] Goodman JW, Lawrence RW. Digital image formation from electronically detected holograms. *Appl Phys Lett* 1967;11:77–9.
- [13] Pedrini G, Tiziani HJ, Zou Y. Digital double pulse-TV-holography. *Opt Laser Eng* 1997;26:199–219.
- [14] Asundi A, Singh VR. Amplitude and phase analysis in digital dynamic holography. *Opt Lett* 2006;31(16):2420–2.
- [15] Pedrini G, Osten W, Gusev ME. High-speed digital holographic interferometry for vibration measurement. *Appl Opt* 2006;45(15):3456–62.
- [16] Fu Y, Pedrini G, Osten W. Vibration measurement by temporal Fourier analyses of digital hologram sequence. *Appl Opt* 2007;46(23):5719–27.
- [17] Wyant JC. Testing aspherics using two-wavelength holography. *Appl Opt* 1971;10(9):2113–8.
- [18] Polhemus C. Two-wavelength interferometry. *Appl Opt* 1973;12(9):2071–4.
- [19] Sodnik Z, Fischer E, Ittner T, Tiziani HJ. Two-wavelength double heterodyne interferometry using a matched grating technique. *Appl Opt* 1991;30(22):3139–44.
- [20] Onodera R, Ishii Y. Time-multiplex two-wavelength heterodyne interferometer with frequency-ramped laser diodes. *Opt Commun* 1999;167:47–51.
- [21] Cheng YY, Wyant JC. Two-wavelength phase shifting interferometry. *Appl Opt* 1984;23(24):4539–43.
- [22] de Groot PJ. Three-color laser-diode interferometer. *Appl Opt* 1991;30(25):3612–6.
- [23] Suzuki T, Kobayashi K, Sasaki O. Real-time displacement measurement with a two-wavelength sinusoidal phase-modulating laser diode interferometer. *Appl Opt* 2000;39(16):2646–52.
- [24] Sasaki O, Sasazaki H, Suzuki T. Two-wavelength sinusoidal phase/modulating laser-diode interferometer insensitive to external disturbances. *Appl Opt* 1991;30(28):4040–5.
- [25] Onodera R, Ishii Y. Two-wavelength laser-diode interferometer with fractional fringe techniques. *Appl Opt* 1995;34(22):4740–6.
- [26] Onodera R, Ishii Y. Two-wavelength interferometry that uses a Fourier-transform method. *Appl Opt* 1998;37(34):7988–94.
- [27] Creath K. Step height measurement using two-wavelength phase-shifting interferometry. *Appl Opt* 1987;26(14):2810–6.
- [28] Schnars U, Jüptner W. *Digital holography: digital hologram recording, numerical reconstruction and related techniques*. Berlin: Springer; 2005.
- [29] Ohlidal M, Sir L, Jaki M, Ohlidal I. Digital two-wavelength holographic interference microscopy for surface roughness measurement. In: *Proc SPIE*. Vol. 5945. 2005, pp. 594501-1-7.
- [30] Pedrini G, Tiziani HJ, Gusev ME. Pulsed digital holographic interferometry with 694- and 347-nm wavelengths. *Appl Opt* 2000;39(2):246–9.
- [31] Kühn J, Colomb T, Montfort F, Charrière F, Emery Y, Cuhe E, et al. Real-time dual-wavelength digital holographic microscopy with a single hologram acquisition. *Opt Express* 2007;15(12):7231–42.
- [32] Goodman JW. *Speckle Phenomena in Optics, Theory and Application*. Ben Roberts 2007.
- [33] Mallat S. *A wavelet tour of signal processing*. 2nd ed. San Diego: Academic Press; 1999.
- [34] Fu Y, Groves RM, Pedrini G, Osten W. Kinematic and deformation parameter measurement by spatio-temporal analysis of an interferogram sequence. *Appl Opt* 2007;46(36):8645–55.